Journal of
Composites Science

Article

Magnetoelectric Effects in Bilayers of PZT and Co and Ti Substituted M-Type Hexagonal Ferrites

Sujoy Saha [1,2], Sabita Acharya [1], Sidharth Menon [1], Rao Bidthanapally [1], Michael R. Page [3], Menka Jain [4] and Gopalan Srinivasan [1,*]

[1] Physics Department, Oakland University, Rochester, MI 48309, USA; sahasujoy3@gmail.com (S.S.); sabitaacharya@oakland.edu (S.A.); sidharthmenon24@gmail.com (S.M.); burao@oakland.edu (R.B.)
[2] Department of Basic Sciences, School of Sciences and Humanities, SR University, Warangal 506371, India
[3] Materials and Manufacturing Directorate, Air Force Research Laboratory, Wright-Patterson Air Force Base, Dayton, OH 45433, USA; michael.page.16@us.af.mil
[4] Department of Physics, University of Connecticut, Storrs, CT 06269, USA; menka.jain@uconn.edu
* Correspondence: srinivas@oakland.edu

Abstract

This report is on Co and Ti substituted M-type barium and strontium hexagonal ferrites that are reported to be single phase multiferroics due to a transition from Neel type ferrimagnetic order to a spiral spin structure that is accompanied by a ferroelectric polarization in an applied magnetic field. The focus here is the nature of magnetoelectric (ME) interactions in the bilayers of ferroelectric PZT and Co and Ti substituted BaM and SrM. The ME coupling in the ferrite-PZT bilayers arise due to the transfer of magnetostriction-induced mechanical deformation in a magnetic field in the ferrite resulting in an induced electric field in PZT. Polycrystalline Co and Ti doped ferrites, $Ba(CoTi)_x Fe_{12-2x}O_{19}$, (BCTx), and $Sr(CoTi)_x Fe_{12-2x}O_{19}$ (SCTx) (x = 0–4) were found to be free of impurity phases for all x-values except for SCTx, which had a small amount of α-Fe_2O_3 in the X-ray diffraction patterns for $x \leq 2.0$. The magnetostriction for the ferrites increased with applied filed H to a maximum value of around 2 to 6 ppm for H ~ 5 kOe. BCTx/SCTx samples showed ferromagnetic resonance (FMR) for x = 1.5–2.0, and the estimated anisotropy field was on the order of 5 kOe. The magnetization increased with the amount of Co and Ti doping, and it decreased rapidly with x for x > 1.0. Measurements of ME coupling strengths were conducted on the bilayers of BCTx/SCTx platelets bonded to PZT. The bilayer was subjected to an AC and DC magnetic field H, and the magnetoelectric voltage coefficient (MEVC) was measured as a function of H and frequency of the AC field. For BCTx-PZT, the maximum value of MEVC at low frequency was ~5 mV/cm Oe, and a 40-fold increase at electromechanical resonance (EMR). SCTx–PZT composites also showed a similar behavior with the highest MEVC value of ~14 mV/cm Oe at low frequencies and ~200 mV/cm Oe at EMR. All the bilayers showed ME coupling for zero magnetic bias due to the magnetocrystalline anisotropy field in the ferrite that provided a built-in bias field.

Keywords: hexagonal ferrites; ferroelectric; multiferroic; magnetoelectric; composite

Academic Editor: Prashanth Konda Gokuldoss

Received: 15 May 2025
Revised: 16 June 2025
Accepted: 24 June 2025
Published: 27 June 2025

Citation: Saha, S.; Acharya, S.; Menon, S.; Bidthanapally, R.; Page, M.R.; Jain, M.; Srinivasan, G. Magnetoelectric Effects in Bilayers of PZT and Co and Ti Substituted M-Type Hexagonal Ferrites. *J. Compos. Sci.* **2025**, *9*, 336. https://doi.org/10.3390/jcs9070336

1. Introduction

Ferrimagnetic hexagonal ferrites are of importance for studies on the nature of magnetic ordering and for a variety of applications for microwave and millimeters wave devices, information storage, and permanent magnets [1–4]. The unique combination of high

Curie temperature, high magnetocrystalline anisotropy field, and insulating properties makes hexagonal ferrites desirable materials for these applications [5,6]. The crystal structure of hexaferrites contains cubic spinel (S-) blocks and two types of hexagonal R- and T-blocks. Depending on the arrangement of the S, R, and/or T-blocks, the ferrites are classified into several types including, M-type ($AFe_{12}O_{19}$), W-type ($AM_2Fe_{16}O_{27}$), X-type ($A_2M_2Fe_{28}O_{46}$), Y-type ($A_2M_2Fe_{12}O_{22}$), Z-type ($A_3M_2Fe_{24}O_{41}$), and U-type ($A_4M_2Fe_{36}O_{60}$), where A is a divalent alkali metal ion (Ba or Sr) and M is usually a divalent or 3d transition metal ion such as Zn, Mg, Co, etc. [7].

Some of the hexaferrites showing ferrimagnetic order are reported to transition to a noncollinear spiral magnetic order under substitutions for A-type or Fe^{3+} ions. When subjected to a moderate magnetic field, they could acquire a transverse-conical spin component that facilitates a magnetic field-driven ferroelectric polarization and are therefore multiferroics [8]. This has prompted extensive investigations on the nature of coupling between the magnetic and ferroelectric orderings in the multiferroic hexagonal ferrites. Multiferroic nature in hexaferrites was first observed in Y-type $Ba_{0.5}Sr_{1.5}Zn_2Fe_{12}O_{22}$ [9], and then in Y-type $Ba_2Mg_2Fe_{12}O_{22}$ [10–12] at low temperatures. Kitagawa et al. [13] reported on cross coupling between the ferroic orderings at room temperature in Z-type $Sr_3Co_2Fe_{24}O_{41}$ [14] which is a type-II multiferroic since the ferroelectricity is magnetic field driven [8]. It is important to note that, for some threshold magnetic fields, the spiral spin structure could become collinear, destroying the induced ferroelectric polarization.

Studies also reveal the existence of a conical spin structure and ferroelectric polarization in several M-type hexagonal ferrites [15,16]. Neutron diffraction studies on barium ferrite, $BaFe_{12}O_{19}$ (BaM), showed evidence for conical spin structure at 1.2 K and the potential to be a type-II multiferroic at low temperatures [15]. When substitution is made at Fe site by Sc and Mg, BaM shows longitudinal conical spin structure at ~30 K [17]. Similarly, Co-Ti substituted BaM and SrM also showed conical spin structure at room temperature [16]. The coupling between the magnetic and ferroelectric subsystems in $Sr(Co,Ti)_xFe_{12-2x}O_{19}$ (SCTx) x = 2 studied by measuring the change in the remnant magnetization M_r under an electric field E showed a 3 % fractional change in M_r for E = 13 kV/cm. Electric field control of magnetization in Co and Ti substituted Sr-hexaferrite was reported by Wang et al., and thin films of the ferrite showed a change in magnetization under the application of a DC electric field [18].

The efforts so far on multiferroic nature of M or Y-type hexaferrites is dedicated to spin induced polarization with the application of moderate magnetic field or E-induced variation in the magnetization. A phenomenon of fundamental and practical importance is the magnetoelectric (ME) effects in a ferrite-ferroelectric composite [19–23]. In such composites, magnetostrictive strain in the ferrite in an applied magnetic field will result in a change in the ferroelectric order parameter and is termed direct-ME (DME) effect [20]. Similarly, converse-ME (CME) effect occurs due to piezoelectric strain in the ferroelectric in an applied electric field that manifests as a change in the magnetization or anisotropy field in the ferrite. The strengths of the ME coupling depend on the magnetostriction λ and piezomagnetic coefficient $q = \delta\lambda/dH$ for the ferrite and the piezoelectric coefficient d for the ferroelectric [20].

The strength of DME in composites could be measured by applying an AC magnetic field h to the composite of thickness t and measuring the resulting AC electric field V. The ME voltage coefficient (MEVC) = V/(ht) is measured as a function of the frequency f of the magnetic field [20]. A bias magnetic field H, however, is essential for the MEVC measurements since the piezomagnetic coefficient q, in most composites, is nearly zero in the absence of H for most of the ferromagnetic materials. Composites of spinel ferrites such as nickel ferrite and cobalt ferrite and ferroelectric PZT or barium titanate have been studied extensively in the past due to their high λ and q-values [20,23–26]. Premkumar et al. [27]

reported strong ME effects in a bilayer of La and Sr co-doped PZT and Zn doped $NiFe_2O_4$ (NZFO).

Ferrite–ferroelectric composites are of importance for a variety of device applications including sensors and actuators, energy harvesting and dual electric field and magnetic field tunable high frequency devices [20,21,25]. However, the need for a bias magnetic field for strong ME coupling is a major technical challenge one has to overcome, in particular for a magnetic sensor array for imaging applications or for energy harvesting. Therefore, a significant effort in the past was the development of composites with self-biased ferromagnetic phases that could eliminate the need for a bias magnetic field [28–30]. A variety of self-biased ME composites have been reported in the past and involved the use of magnetization graded ferromagnetic phase, composition graded spinel ferrites, or the use of a ferromagnetic phase with a large magnetocrystalline anisotropy field.

The current study was motivated by reports on strong ME effects under self-bias in composites with M-type hexagonal ferrites [31–33]. Hexagonal BaM and SrM have uniaxial anisotropy fields H_A on the order of 17–18 kOe, and one expects a magnetic bias arising out of the large H_A leading to a strong ME coupling in the absence of an external bias. Although the multiferroic properties of Co-Ti substituted BaM and SrM have been studied extensively, their strain mediated ME coupling in a bilayer with a ferroelectric is yet to be investigated. We report here results of our studies on bilayers of PZT and M-type Ba and Sr ferrites with Co and Ti substitutions, $Ba(CoTi)_xFe_{12-2x}O_{19}$ (BCTx) and $Sr(CoTi)_xFe_{12-2x}O_{19}$ (SCTx) ($x = 0$–4.0). Vendor supplied PZT and ferrites prepared by ceramic techniques were used. Polycrystalline ferrites were characterized in terms of structural parameters by X-ray diffraction and scanning electron microscopy (SEM). Magnetization M measurements showed an increase in M up to $x = 1.0$ and then a monotonic decrease for $x > 1.0$. Magnetostriction was found to be significantly higher than for SrM or BaM. A large magnetocrystalline anisotropy field in the ferrites was inferred from FMR observed in samples with $x > 2$. Ferrite-PZT bilayers made by bonding techniques were used for studies on the direct-ME (DME) effect, i.e., the influence of magnetic fields on ferroelectric order parameters. The ME voltage coefficient (MEVC) was measured at low frequencies and at electromechanical resonance (EMR). ME coupling under self-bias and strengthening of the coupling strengths at EMR were evident from the measurements on the bilayers. Further details are provided in the sections that follow.

2. Experiment

Polycrystalline Co and Ti substituted M-type hexaferrites, BCTx and SCTx ($x = 0$–4.0, in steps of 0.5), were synthesized by traditional solid state reaction techniques. Precursor materials viz, $Ba/SrCO_3$, $CoCO_3$, TiO_2 and Fe_2O_3 were mixed in a wet ballmill for 8 h. The slurry was air dried and presintered at 900 °C for 6 h followed by a second ballmilling for 8 h. After drying, the powder was mixed with a binder. Disc shaped samples, 15 mm in diameter, were pressed in a die under a uniaxial pressure of 2 MPa. The final sintering was carried out in air at 1200–1250 °C for 6 h.

The crystal structure and phase purity were investigated with a powder X-ray diffractometer (Rigaku, Tokyo, Japan). The morphological features of the samples were studied using a scanning electron microscope (SEM) (JEOL, Tokyo, Japan). Magnetization of the samples as a function of magnetic field up to 5 kOe was measured at room temperature with a Faraday susceptibility balance (Cahn, Paramount, USA). Magnetostriction λ was measured on thin rectangular platelets of the samples by attaching a strain gage. The in-plane λ parallel to the applied magnetic field direction was measured with a strain indicator. Ferromagnetic resonance (FMR) measurements were conducted on thin rectangular platelets of the composites. The samples were placed in an S-shaped coplanar wave guide with an external field H parallel to the plane of the sample. We used a vector network analyzer (Agilent, Santa Clara, USA) to record profiles of the scattering matrix S_{21} vs. frequency for a series of H.

Ferrite-PZT bilayers for measurements of direct-ME effects were made by bonding vendor supplied PZT (APC-850, American Piezo Ceramics, PA, USA) with a two-part epoxy (M-bond 600, Vishay, Raleigh, USA). The bonding procedure involved applying a thin layer of the epoxy to ferrite and PZT layers, followed by curing the epoxy by heating the bilayer to 125 °C. The thickness of the epoxy layer was kept to a minimum, 5 to 10 µm, so that it had no adverse effects on the transfer of mechanical deformation at the PZT-ferrite interface. The ME voltage coefficient (MEVC) of the bilayer composites was measured by applying a DC field H with an electromagnet and an AC magnetic field h of frequency f generated with a pair of Helmholtz coils. The magnetic fields were parallel to each other and either parallel or perpendicular to the sample plane. The ME voltage (V) generated across PZT was measured with a lock-in-amplifier. The ME voltage coefficient MEVC = (V/t h), where t is the thickness of PZT, was measured as function of H as well as the frequency f of AC field.

3. Results

3.1. Structural Characterization and Morphological Features

X-ray diffraction patterns for BCTx and SCTx are shown in Figure 1a,b, respectively. The intensity peaks for BCTx in Figure 1a were identified with the M-type hexagonal ferrite BaM (shown in the bottom pane) and did not reveal any impurity phases. For SCTx, the patterns in Figure 1b (and Figure S1 in the Supplementary Materials) show, in addition to peaks due to M-type ferrite, a weak peak corresponding to α-Fe_2O_3 for $x \leq 2.0$. Similar impurities in SrM were also reported for samples prepared by different techniques [33]. For $x > 2.0$, however, the XRD patterns are free of any impurity phase and dilution of the Fe^{3+} content by Co^{2+} and Ti^{4+} may be the cause of absence of α-Fe_2O_3. The weight fraction of the impurity phase, α-Fe_2O_3, was 4.74% for SCT0.0 and 4.56% for SCT2.0. Bulk α-Fe_2O_3 is an antiferromagnet and the small amount of it in SCTx is unlikely to influence the magnetic order parameters of the hexaferrite [34].

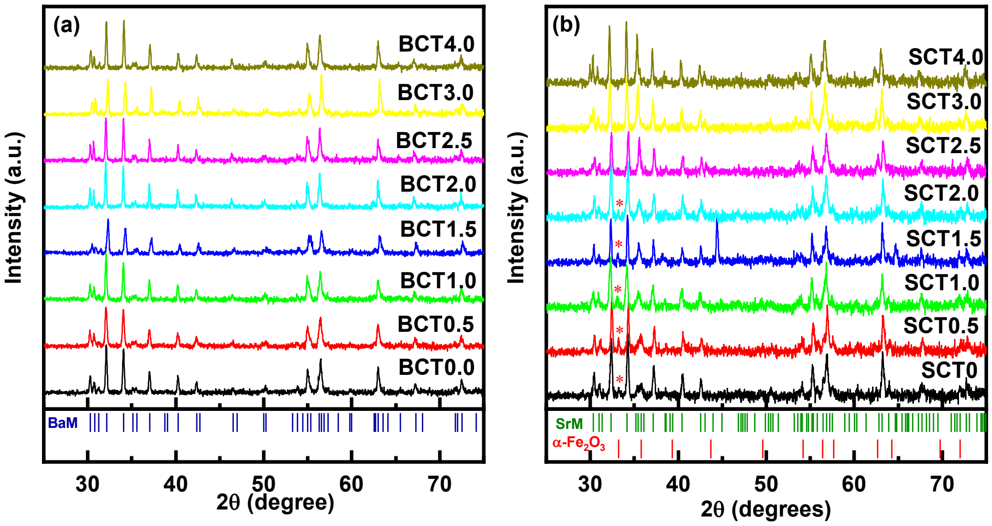

Figure 1. X-ray diffraction patterns for (**a**) BCTx and (**b**) SCTx. The stick patterns for BaM (blue) are shown in the bottom pane of (**a**). Patterns for SrM (green) and α-Fe_2O_3 (red) are shown in the bottom pane of (**b**). Peaks of α-Fe_2O_3 in SCTx for $x \leq 2.0$ are denoted by the asterisk symbol in (**b**).

Figure 2 shows representative SEM images of surface features for the BCTx/SCTx samples. Pure BaM/SrM (x = 0.0) shows very small grains (~1 μm). Figure 2b–d for BCTx also show needle shaped grains with the grain size increasing with increasing x.

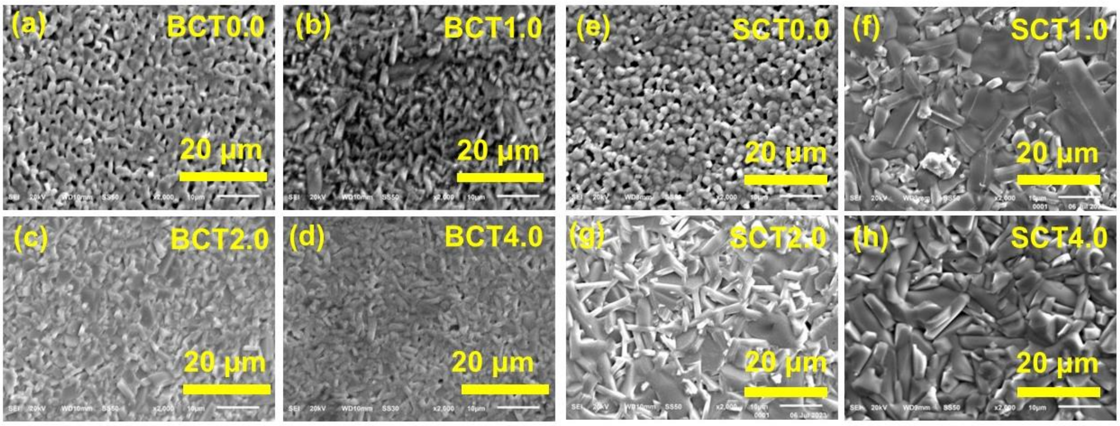

Figure 2. SEM images of grains in (**a**–**d**) for polycrystalline BCTx and (**e**–**h**) for SCTx (x = 0.0, 1.0, 2.0 and 4.0).

For SCTx samples, very small grains (~1 μm) are seen in Figure 2e for x = 0. With increasing x, the images show both small and large grains (~15 μm), and SCTx samples have a larger grain compared to BCTx. The microstructures of both BCTx and SCTx show significant variations with the amount of substitution x and will influence the magnetic field H-dependence of the magnetostriction λ [35]. Since the ME voltage coefficient is directly proportional to the piezomagnetic coefficient q = dλ/dH and its H-dependence tracks the variation in q with H, one anticipates a direct influence of the microstructure on the ME response of the ferrite-PZT bilayer.

3.2. Magnetization

We used a Faraday susceptibility balance to measure the room-temperature magnetization M of the samples as a function of magnetic field H. Figure 3 shows the data for BCTx. Although saturation of M is expected to occur at fields as high as 20 kOe for BaM [36], the figure shows M vs. H M for the maximum available field of 5 kOe in our Faraday balance. In Figure 3, one observes the typical ferromagnet-like behavior with an increase in M with H for x = 0.5 and 4πM value for H = 5 kOe increases from 3.29 kG for BCT0.5 to 4.22 kG for BCT1.0. With a further increase in x, the magnetization shows a rapid decrease, from 3.38 kG for BCT1.5 to 0.38 for BCT2.5 that is caused by replacing Fe^{3+} with the dopants Co, a low magnetic moment 3d ion, and nonmagnetic Ti. For x > 1.5, the dramatic fall off in M-values is due to transition in the magnetic structure from ferrimagnetic Neel type to spiral spin structure.

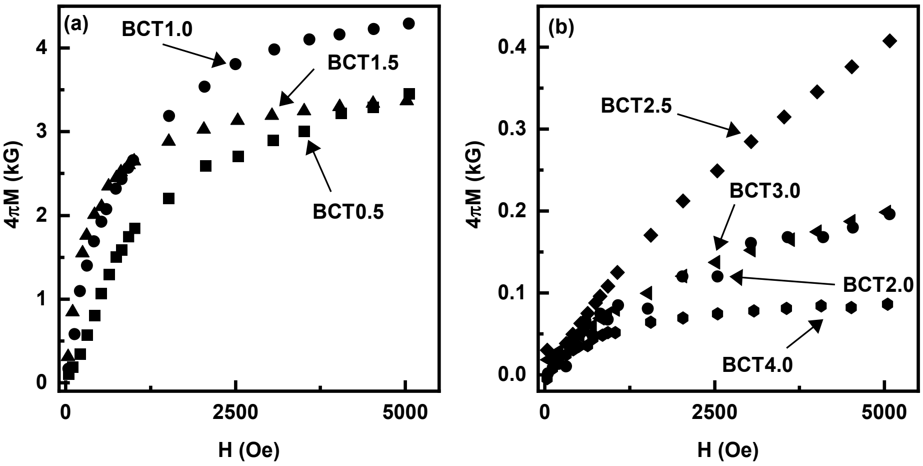

Figure 3. Magnetization 4πM vs. H data for BCTx for **(a)** x = 0.5–1.5 (**a**) and x = 2.0–4.0 (**b**).

Similar magnetization data for SCTx are shown in Figure 4. For SCT0.5, the M-H loop mostly overlaps with that of SCT0.0 (or pure SrM). When doping is increased to x = 1.0, a higher 4 πM of 3.61 kG is measured at H = 4.5 kOe, compared to 2.54 kG at H = 4.5 kOe for SCT0.5. The site preference of the dopants, Co and Ti, causes this increase in M [37,38]. Mössbauer spectroscopy measurements have shown that Co^{2+} has a preference to occupy the octahedral $4f_2$ crystallographic site when substituted for Fe^{3+}. The occupation of Co^{2+} in $4f_2$ sites will reduce the amount of magnetic moment directed opposite to the net moment direction causing an increase in the total magnetic moment [39]. As the doping increases, the Fe sites are replaced by nonmagnetic Ti as well as magnetic Co creating a magnetic arrangement wherein net magnetic moment decreases. The contribution from α-Fe_2O_3 impurities for $x \leq 2.0$ is insignificant as its magnetization is rather small [34].

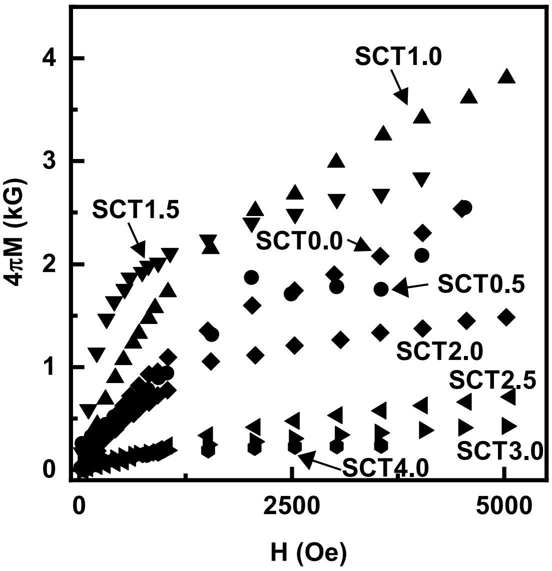

Figure 4. Magnetization 4πM vs. H for SCTx for x = 0.5–4.0.

3.3. Magnetostriction

The magnetostriction λ of BaM/SrM is rather low, ~1 ppm for H-values on the order of 3 kOe, and the piezomagnetic coefficient q is also very small, making them not suitable for obtaining strong ME coupling in a composite with a ferroelectric [31,40]. It is to be noted that for SCTx ($x \leq 2.0$), α-Fe_2O_3 impurities will not affect the overall magnetostriction since its weight fraction too small (<5%). The H-dependence of λ for BCTx/SCTx samples are shown in Figure 5 (and Supplementary Materials Figure S2). The data are for measurements parallel to in-plane H for a rectangular platelet. For BCT0.5, λ is positive (Supplementary Materials Figure S2). All other BCTx compositions show negative magnetostriction with no systematic variation of the magnetostriction over the composition range. The highest magnetostriction, −6 ppm, is measured for BCT1.0 at 2.5 kOe as shown in Figure 5a. SrM shows a negative magnetostriction of −3 ppm, (Supplementary Materials Figure S2). However, a positive magnetostriction for SrM single crystal was reported in the past [24]. With an increase in the Co and Ti content, λ increases to −4 ppm for SCT3.0 at 2.5 kOe (Figure 5f).

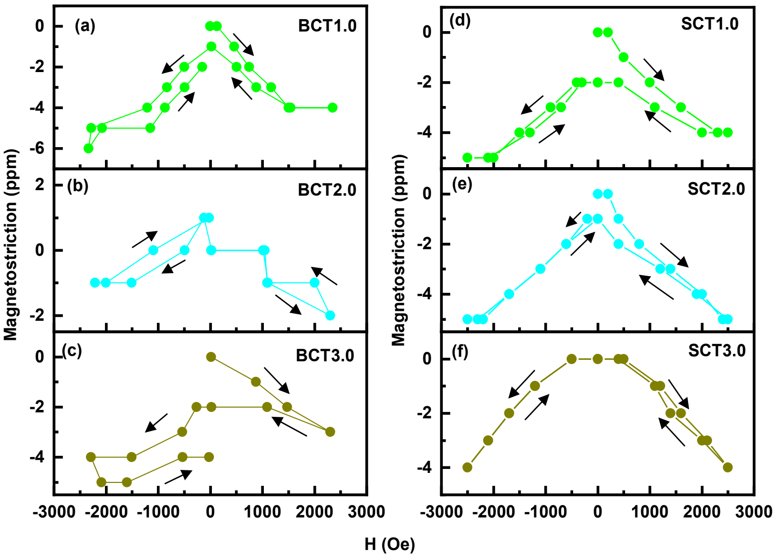

Figure 5. Magnetostriction vs. H for (**a**–**c**) BCTx and (**d**–**f**) SCTx samples. The data are for measurements parallel to the applied in-plane magnetic field.

3.4. Ferromagnetic Resonance

FMR measurements were conducted on thin rectangular platelets of the ferrites to determine the magnetocrystalline anisotropy. The samples were placed in an S-shaped coplanar waveguide and excited with microwave power from a VNA. With a static magnetic field H applied parallel to sample plane, profiles of the scattering matrix S_{21} as a function of frequency f and H were recorded. In BCTx samples, FMR was observed only for a narrow composition, for $x = 1.5$–2.0, as shown in Figure 6a,b. For $x < 1.0$, BCTx samples showed absorption peaks for $f > 40$ GHz (Supplementary Materials Figure S3), and we identified them with the excitation of a magneto-dielectric mode for the following reason. Estimates on the rate of change of the mode frequency f_r with H yielded ~1.5 MHz/Oe for BCT0.5. For FMR modes, however, one expects a value close to the gyromagnetic ratio $\gamma \sim 2.7$–3.0 MHz/Oe [40]. The slow rate of increase in f_r with H for modes above 40 GHz indicates that they are magneto-dielectric modes [41] and are not considered here for further analysis.

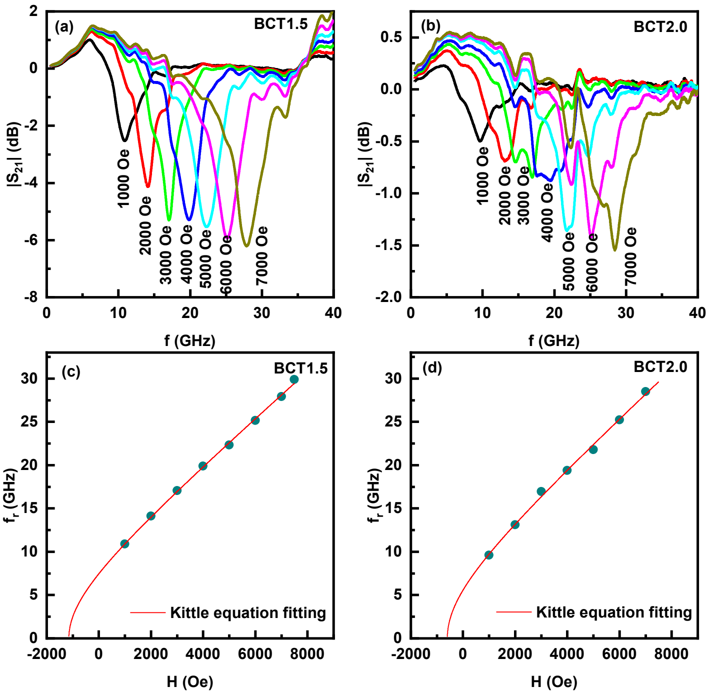

Figure 6. Profiles of S_{21} vs. f showing resonance in (**a**) BCT1.5 and (**b**) BCT2.0. The profiles are for in-plane H. Fitting of the FMR data on f_r vs. H to Equation (1) are shown in (**c**,**d**).

The FMR mode frequency f_r as a function of H for BCT1.5 and BCT2.0 are plotted in Figure 6c,d, respectively. We fitted the data to the Kittel equation.

$$f_r = \gamma\left(\left(H + (N_z - N_x)4\pi M_{eff}\right)\left(H + \left(N_y - N_x\right)4\pi M_{eff}\right)\right)^{1/2} \quad (1)$$

Here, H is the applied magnetic field along the sample length (x-direction), N_x, N_y, and N_z are the demagnetization factors along the length, width, and thickness of the platelet, respectively, and $4\pi M_{eff} = 4\pi M + H_A$, where $4\pi M_{eff}$ is the effective magnetization of the specimen and H_A is magnetocrystalline anisotropy. For estimates of H_A from $4\pi M_{eff}$, one has to use the value of $4\pi M$ at H corresponding to f_r since the samples do not show saturation of M for H up to 5 kOe as seen in Figure 4. Figure 6c,d shows the fitting of mode frequency f_r versus H for values for γ, $4\pi M_{eff}$, and H_A listed in Table 1.

Table 1. Fitting parameters of the FMR absorption for BCTx and SCTx samples.

Sample	Fitting Parameters			
	γ (MHz/Oe)	$4\pi M_{eff}$ (kG)	$4\pi M$ (kG) from Figure 4	H_A (kOe)
BCT1.5	2.63	9.46	3.29	6.17
BCT2.0	2.75	8.19	0.17	8.02
SCT1.5	2.80	7.74	2.84	4.90
SCT2.0	3.08	6.37	1.27	5.10

Similar S_{21} vs. f profiles for SCTx ($1.5 \leq x \leq 2.0$) are shown in Figure 7a,b and in Supplementary Materials Figure S4 for $x < 1.5$ and $x > 2.0$. The magnetic parameters obtained from fitting of f_r vs. H data for SCTx are listed in Table 1. In addition to FMR for the above x-values, magneto-dielectric modes were observed at frequencies above 40 GHz [41,42]. It is important to note here that H_A is indeed an in-plane anisotropy field in the polycrystalline samples of Co and Ti substituted BaM and SrM. Single crystal SrM and BaM have uniaxial anisotropy fields of 17–18 kOe, and one may infer from the in-plane H_A values in

Table 1 for BCTx and SCTx that a majority of the randomly oriented grains in the samples have the hexagonal c-axis perpendicular to sample plane [43,44]. It is also noteworthy that H_A value increases with increasing the x value for both BCTx and SCTx for $1.5 \le x \le 2.0$ and the highest $H_A = 8.02$ kOe is obtained for BCT2.0.

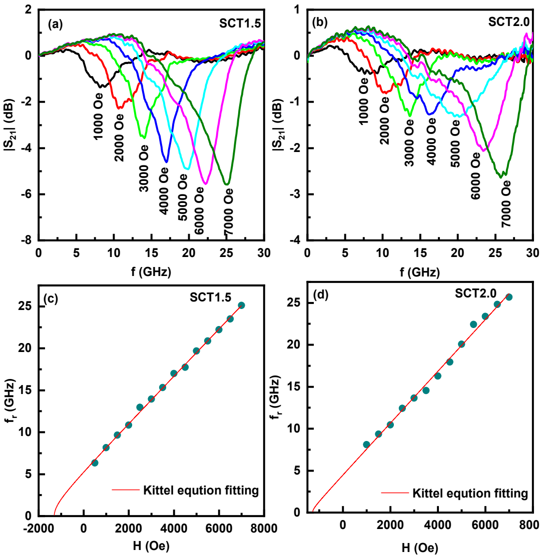

Figure 7. Profiles of S_{21} vs. f showing resonance in (**a**) SCT1.5 and (**b**) SCT2.0 for in-plane static magnetic fields. Fitting of the FMR data on f_r vs. H to Equation (1) are shown in (**c**,**d**).

3.5. ME Effects in Bilayers of BCTx/SCTx and PZT

The most important aspect of this report is the studies on strain mediated direct-ME effects, i.e., the influence of applied magnetic fields on ferroelectric order parameters, in bilayers of the ferrites and PZT. Bilayers of ferrite-PZT were made with vendor supplied pre-poled PZT (APC PZT #850) with silver electrodes. Rectangular platelets of the ferrite (10 mm × 5 mm × 0.5 mm) were bonded to PZT (12 mm × 5 mm × 0.3 mm) with a thin layer (~ 5 mm) of a 2-part epoxy as described earlier. The sample was placed in a metal box to eliminate RF and any other source of noise. A pair of Helmholtz coils inside the box was used to generate an AC magnetic field h at frequency f and an electromagnet was used to apply a static field H, with both fields parallel to each other. The ME voltage V produced across the thickness of PZT was measured with a lock-in amplifier. The magnetoelectric voltage coefficient MEVC = V/(h × t), where t is the thickness of the PZT, was measured as function of H or f for the following conditions: α_{31} for H and h parallel to the sample length (direction 1) and V measured across PZT (direction 3) and α_{33} for both magnetic fields perpendicular to bilayer plane and V measured across PZT thickness.

The variations in α_{31} and α_{33} with H are shown in Figures 8 and 9, respectively, for BCTx (x = 0, 2.0, 4.0)-PZT for h = 1 Oe at 100 Hz. Data for other BCTx-PZT bilayers are shown in Supplementary Materials Figure S5. Significant features in the data in Figures 8 and 9 are as follows. (i) The composites show a relatively large MEVC under zero external bias, i.e., H = 0. (ii) The MEVC vs. H shows hysteresis and remanence, and (iii) BCTx-PZT composites show a much smaller maximum MEVC, as much as two orders of magnitude, compared to spinel ferrite–ferroelectric composites [20].

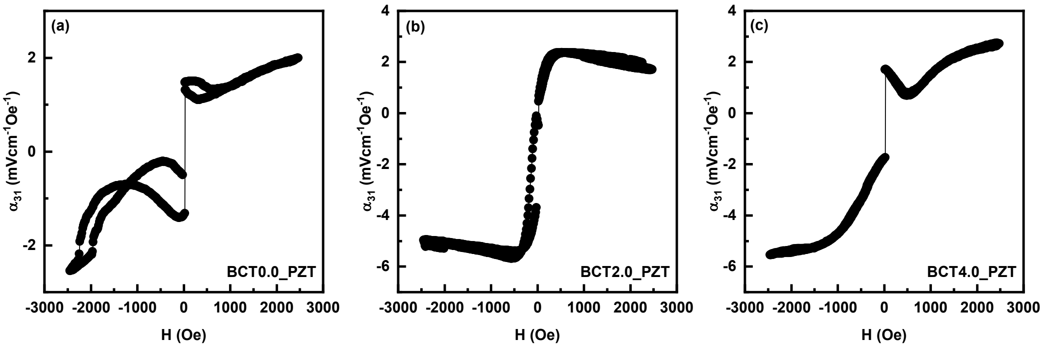

Figure 8. α_{31} vs. H for the PZT-BCTx (x = 0.0, 2.0, 4.0) bilayers.

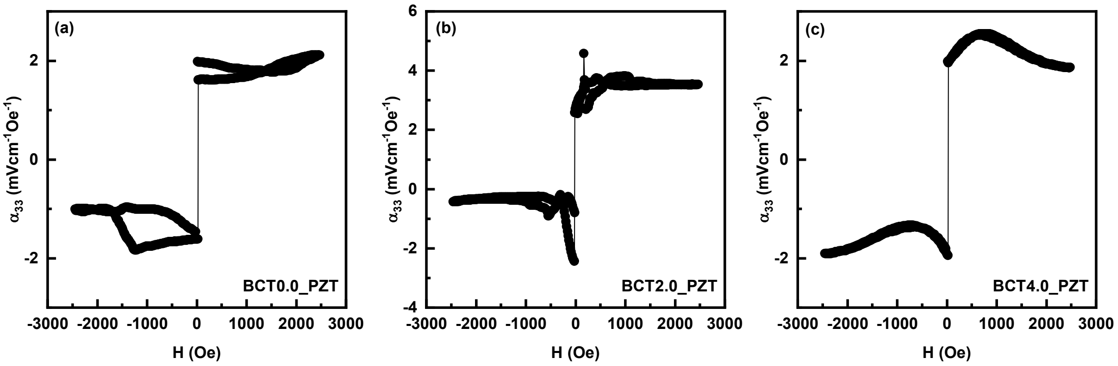

Figure 9. α_{33} vs. H for PZT-BCTx (x = 0.0, 2.0, 4.0) bilayers.

In the case of ferromagnetic transition metals and alloys and spinel ferrites, the magnetostriction λ at low H-values is proportional to M^2, and both λ and q will increase slowly from near-zero value with increasing H. Therefore, MEVC, which is directly proportional to q, will be very small or zero for H = 0 [20]. The non-zero values of MEVC in Figures 8 and 9 for BCTx-PZT could be attributed to the large H_A values in the BCTx that act as a built-in magnetic bias leading to a large MEVC. It is worth noting that all the BCTx-PZT composites show zero-bias MEVC as seen in the data of Figures 8 and 9 (and Supplementary Materials Figure S5). There is also asymmetry in the MEVC vs. H data except for α_{31} for BCT2.0-PZT (Figure 8c) that also has the highest MEVC ~5.7 mV/cm Oe. One anticipates a smaller α_{33} compared to α_{31} due to demagnetization associated with DC and AC magnetic fields perpendicular to the bilayer plane. However, the data in Figures 8 and 9 do not indicate the expected weakening in the magnitude of α_{33}.

Results of similar MEVC vs. H data for the bilayers of SCTx-PZT are shown in Figures 10 and 11. The bilayer of SCT0.0-PZT shows monotonically increasing α_{31} with H (Figure 10a) and an almost constant, H-independent α_{33} as seen in the data of Figure 11a. The MEVC values for SCT0.0-PZT are higher than reported values for the bilayers of single crystalline SrM and PZT [31]. For the SCT2.0-PZT, α_{31} increases with H to a maximum of 14 mV/cm Oe, the highest value for the bilayers studied in this work (Figure 10b and Supplementary Materials Figure S6). The large piezomagnetic coefficient q of SCT2.0 results in the highest MEVC for SCT2.0-PZT bilayer. Data on α_{33} vs. H in Figure 11b show a decrease in the MEVC value compared α_{31} due to demagnetization effects for out-of-plane magnetic fields. All of the SCTx-PZT show a similar lowering of α_{33} values with respect to their α_{31} value, (Supplementary Materials Figure S6).

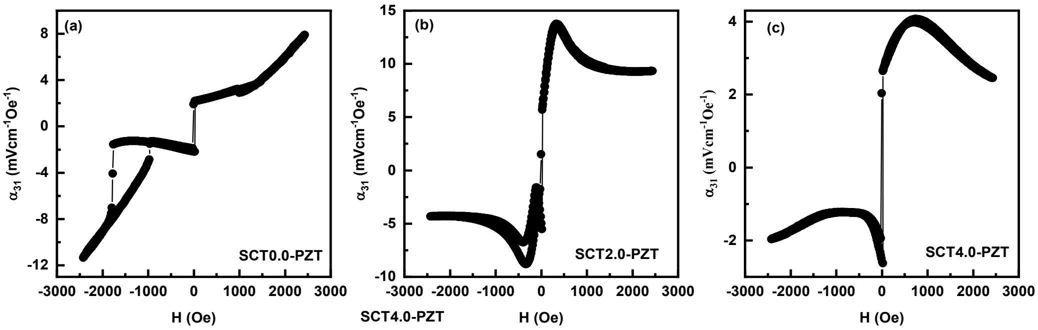

Figure 10. α_{31} vs. H for PZT-SCTx (x = 0.0, 2.0, 4.0) bilayers.

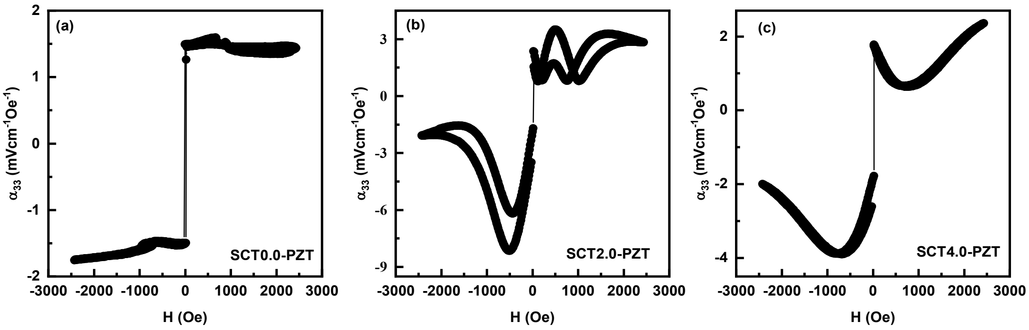

Figure 11. α_{33} vs. H for PZT-SCTx (x = 0.0, 2.0, 4.0) bilayers.

Studies on the dependence of MEVC on the frequency f of the AC magnetic field are important since one expects significant enhancement in the MEVC values when f coincides with the frequency of the acoustic resonance modes [20]. We carried out the MEVC measurement at the electromechanical resonance (EMR) in the BCTx/SCTx-PZT samples. The EMR mode frequencies were first measured by f-dependence of the capacitance of the bilayer with an LCR meter. Then, the MEVC α_{31} of the bilayers was measured as a function of f in the vicinity of the EMR for each sample. A bias magnetic field corresponding to the maximum in low-frequency MEVC was applied during these measurements. Data on α_{31} vs. f for BCTx/SCTx-PZT bilayers are shown in Figure 12 (and in Supplementary Materials Figure S7). A significant enhancement of MEVC compared to low-frequency values was measured for all the samples. Among the BCTx-PZT bilayers, the highest MEVC of 205 mV/cm Oe at EMR was measured for BCT0.5-PZT and is a factor of 40 higher than for the low-frequency α_{31}. Similarly, among the SCTx-PZT bilayers, the highest MEVC of 204 mV/cm Oe at EMR was measured for SCT2.0-PZT. The enhancement of MEVC at EMR is more prominent in SCTx-PZT samples than BCTx-PZT samples as seen in the Supplementary Materials Figure S7. The maximum values of MEVC at low frequency and at EMR are shown in the Supplementary Materials Figure S8.

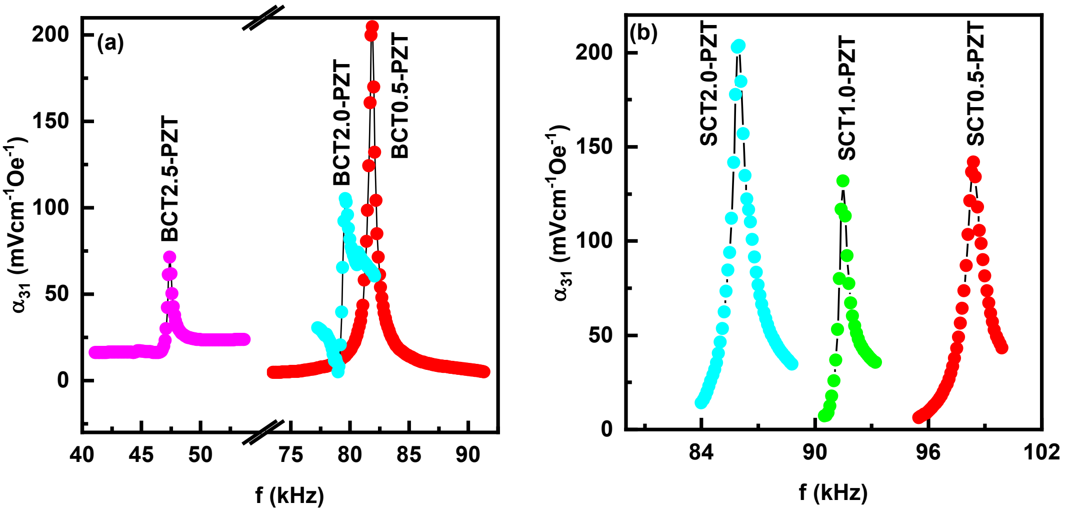

Figure 12. MEVC as a function of frequency of the AC magnetic field for bilayers of (**a**) BCTx-PZT and (**b**) SCTx-PZT. The peak values occur at the frequency of longitudinal acoustic modes in the bilayers.

4. Discussion

It is well established that Co and Ti doped BaM and SrM with conical spin structure are multiferroic showing cross coupling between the magnetic and ferroelectric subsystems [8]. The primary focus of this study was to investigate the ME coupling arising due to magnetostriction induced mechanical deformation in applied magnetic fields in composites of PZT and Co-Ti substituted BaM/SrM. Incorporation of the Co and Ti in BaM/SrM does not in most cases lead to impurity phases, except for in SCTx for $x < 2.0$ with less than 5 wt.% of a-Fe_2O_3. The polycrystalline samples are found to have a uniaxial magnetocrystalline anisotropy field H_A for $x < 2.0$ and an in-plane H_A for higher x-values. The large uniaxial anisotropy (>15 kOe) in single crystal BaM and SrM [3] reduces to an in-plane H_A in polycrystalline BCTx/SCTx for $x > 2.0$. This reduction in anisotropy is also evident in the magnetization $4\pi M$ vs. H data in Figure 4. Within the limited range of H-values, there is an ease for M to reach towards saturation as x is increased from BCT0.0/SCT0.0 to BCT4.0/SCT4.0.

Somewhat minor variations appear in the MEVC with the substitution x in BCTx/SCTx-PZT composites both at low frequencies and at EMR. The ME coupling strengths in SCTx-PZT is stronger than for BCTx-PZT and can be attributed to higher value of the magnetostriction λ and the piezomagnetic coefficient q (Figures 5 and S2 Supplementary Materials). It is also noteworthy that the maximum zero-bias MEVC at low frequency and at EMR occurs for $x = 2.0$ for both bilayer systems (Figure S8 Supplementary Materials) that could very well be attributed to the higher H_A value than for other substitutions.

Samples of BCTx/SCTx show only a moderate value of magnetostriction, much smaller than for the bilayers of PZT and spinel ferrites such as nickel ferrite (NFO) or cobalt ferrite (CFO), but higher than for samples with BaM or SrM. Thus, the overall strengths of the direct-ME coupling in the bilayers of BCTx/SCTx with PZT are one to two orders of magnitude smaller than for NFO/CFO-PZT [20], but a large magnetocrystalline anisotropy field gives rise to significant zero-bias MEVC in BCTx/SCTx-PZT. At frequencies corresponding to longitudinal acoustic modes, the MEVC values show enhancement by a factor of 40 or so compared to low-frequency values. Since the ME effect in the composites arises from the mechanical coupling between the piezoelectric and magnetic phases, the ME response can be significantly amplified when the piezoelectric component experiences resonance, particularly electromechanical resonance [20]. Guerra et al. [45] have reported on particulate composites comprising BaM and PZT and an MEVC of ~95 mV/cm Oe near EMR whereas our samples show twice the value. Single crystal SrM-PZT bilayer was reported to show MEVC ~5 mV/cm Oe around 3 kOe [31], much smaller than for our SCTx-PZT samples.

A variety of layered composites containing ferrites, 3d-rare earth and transition metals/alloys, or manganites for the ferromagnetic phase and PZT, barium titanate, or lead magnesium niobate-lead titanate (PMN-PT), were studied in the past and several of them show evidence for strong ME coupling. Next, we compared the strength of ME coupling in BCTx/SCTx-PZT bilayers with similar bilayer composites. Palneedi et al. reported a maximum MEVC of 3 V/cm Oe for PZT-Metglas bilayers [46]. A much higher MEVC of 4.68–5.9 V/cm Oe was reported for terfenol D-PZT bilayers [47,48]. An MEVC of 12 V/cm Oe was measured in a bilayer of P(VDF-HFP)-Metglas [49]. Composites of NFO or CFO and PZT in general have a MEVC of 400 mV/cm Oe much lower compared to composites with ferromagnetic metals or alloys [20].

The origin of magnetic control of ferroelectricity in doped multiferroic BaM and SrM is well established but the nature of strong of magnetocrystalline anisotropy and moderate magnetostriction in polycrystalline samples of Co-Ti substituted BaM/SrM need to be understood. The key finding of this study on BCTx/SCTx-PZT are the ME coupling under zero external bias and MEVC as high as ~200 mV/cm Oe at EMR mode frequencies. In this regard, studies on H_A and magnetostriction for Co/Ti doping higher than 4.0 in BaM/SrM are of interest for enhancing the strengths of ME coupling at low frequencies and at EMR and also strengthening the zero-bias ME effects.

The bilayer ME composites studied here have a rather weak ME coupling strength in the low frequency regime. The ME response in the vicinity of electromechanical resonance shows a larger MEVC~200 mV/cm Oe. This large value of MEVC of these bilayers under zero-bias is of potential interest for use in magnetic field sensors and sensor arrays. Energy harvesting is another possible device application for the composites. The hexaferrites show FMR at 10–30 GHz for H = 1–7 kOe and the composites may have the potential for FMR-based devices such as resonators and filters, and composites with PZT may facilitate electric field tuning of the operating frequencies of such devices.

5. Conclusions

The nature of magnetoelectric interactions has been studied in the bilayers of Co-Ti substituted M-type barium and strontium hexagonal ferrites and PZT. Even though BCTx and SCTx are single phase multiferroics showing coupling between magnetic and ferroelectric order parameters, studies on ME coupling due to magnetostriction in the ferrites and piezoelectric effects in PZT have not been addressed so far. Samples of BCTx prepared by solid state reaction techniques are free of impurity phases, whereas a minor amount of α-Fe_2O_3 phase was present in SCTx only for $x < 2.0$. SEM images show small, irregular shaped grains and needles like structures and an increase in the grain size was observed with increase in x. Magnetostriction at room temperature values for H up to 5 kOe were much higher than the reported values for single crystal BaM and SrM. Magnetization data for H up to 5 kOe indicated an initial increase M with x up to 1.0, but a sharp decrease in M was measured for higher x-values. The magnetocrystalline anisotropy of the samples estimated by FMR revealed a switch from out-of-plane to in-plane H_A as the amount of Co-Ti substitution was increased with an in-plane H_A of 5 kOe for SCT1.5 and 2.0. Low-frequency and resonance ME voltage coefficient measurements were conducted on the bilayers of BCTx/SCTx-PZT. The maximum values of low-frequency MEVC ranged from a minimum of 2 mV/cm Oe to a maximum of 14 mV/cm Oe and are two orders of magnitude smaller than for spinel ferrite–PZT composites. A key observation in this study is the zero-bias field ME effects that could be attributed to a large H_A in the ferrites that acts as a built-in bias. The MEVC was as high as 200 mV/cm Oe when the frequency of the AC magnetic field coincides with acoustic resonance modes in the composites.

Supplementary Materials: The following supporting information can be downloaded at: https://www.mdpi.com/article/10.3390/jcs9070336/s1. Figure S1. Rietveld refinement of the XRD pattern of (a) SCT0.0 and (b) SCT2.0. Both the systems contain hexagonal M-type ferrite phase with $P6_3/mmc$ space group symmetry (shown in green Braggs' positions) and α-Fe_2O_3 phase with R-3c space group symmetry (shown in purple Braggs' positions). Figure S2. Magnetic field dependence of the magnetostriction of (a) BCTx and (b) SCTx samples. Figure S3. S_{21} vs. f profiles of different BCTx samples at selected magnetic fields. Figure S4. S21 vs. f profiles of different SCTx samples at selected magnetic fields. Figure S5. MEVC for BCTx-PZT bilayers for in-plane and out-of-plane magnetic fields. Figure S6. MEVC for SCTx-PZT bilayers for in-plane and out-of-plane magnetic fields. Figure S7. MEVC plots of (a) BCTx-PZT and (b) SCTx-PZT bilayer composite samples as a function of frequency near EMR. In the inset of (b) the variation of the capacitance of PZT layer attached to the SCT2.0-PZT bilayer is shown. Figure S8. Zero-bias MEVC, MEVC at EMR and maximum achievable MEVC in field scan for SCTx-PZT bilayer composites. Table 1. Fitting parameters of the FMR absorption for BCTx and SCTx samples.

Author Contributions: S.S., S.A., S.M., and R.B. were involved in sample synthesis and structural, magnetic, and magnetoelectric characterization. S.S., M.R.P., M.J., and G.S. contributed to data analysis, manuscript preparation, project management, and funding acquisition. All authors have read and agreed to the published version of the manuscript.

Funding: The research at Oakland University was supported by grants from the National Science Foundation (ECCS-2415328, ECCS-EAGER-2236879) and the Air Force Research Laboratory (Award No. FA9550-23RXCOR001). Efforts at the University of Connecticut were supported by the NSF (ECCS-EAGER-2236879). The research at AFRL was supported by a grant from the Air Force Office of Scientific Research (AFOSR Award No. FA9550-23RXCOR001).

Data Availability Statement: All data generated or analyzed during this study are included in this published article [and its Supplementary Information Files].

Conflicts of Interest: The authors declare no conflicts of interest.

References

1. Tkachenko, M.V.; Ol'khovik, L.P.; Kamzin, A.S. Magnetic ceramics based on hydroxyapatite modified by particles of M-type hexagonal ferrite for medical applications. *Phys. Solid State* **2011**, *53*, 1588–1593.
2. Belous, A.G.; Solovyova, E.D.; Solopan, S.O.; Yelenich, O.V.; Bubnovskaya, L.N.; Osinsky, S.P. Properties and potential applications of ferromagnetic nanostructures in medicine and microwave engineering. *Solid State Phenom.* **2015**, *230*, 95–100.
3. Pullar, R.C. Hexagonal ferrites: A review of the synthesis, properties and applications of hexaferrite ceramics. *Progr. Mater. Sci.* **2012**, *57*, 1191–1334.
4. Wohlfarth, E.P. Ed; *Ferromagnetic Materials*; North-Holland Publishing Company: Amsterdam, The Netherlands, 1980; Volume 2.
5. Smit, J.; Wijn, H.P.J. *Ferrites*; Phillips Technical Library: Eindhoven, The Netherlends, 1959.
6. Sugimoto, M. The past, present, and future of ferrites. *J. Am. Ceram. Soc.* **1999**, *82*, 269–280.
7. Brawn, R.B. The crystal structure of a new group of ferromagnetic compounds. *Philips Res. Rep.* **1957**, *12*, 491–548.
8. Kimura, T. Magnetoelectric hexaferrites. *Annu. Rev. Condens. Matter Phys.* **2012**, *3*, 93–110.
9. Kimura, T.; Lawes, G.; Ramirez, A.P. Electric polarization rotation in a hexaferrite with long-wavelength magnetic structures. *Phys. Rev. Lett.* **2005**, *94*, 137201.
10. Ishiwata, S.; Taguchi, Y.; Murakawa, H.; Onose, Y.; Tokura, Y. Low-magnetic-field control of electric polarization vector in a helimagnet. *Science* **2008**, *319*, 1643–1646.

11. Taniguchi, K.; Abe, N.; Ohtani, S.; Umetsu, H.; Arima, T.H.; Ferroelectric polarization reversal by a magnetic field in multiferroic Y-type hexaferrite $Ba_2Mg_2Fe_{12}O_{22}$. *Appl. Phys. Express* **2008**, *1*, 031301.
12. Ishiwata, S.; Okuyama, D.; Kakurai, K.; Nishi, M.; Taguchi, Y.; Tokura, Y. Neutron diffraction studies on the multiferroic conical magnet $Ba_2Mg_2Fe_{12}O_{22}$. *Phys. Rev. B* **2010**, *81*, 174418.
13. Kitagawa, Y.; Hiraoka, Y.; Honda, T.; Ishikura, T.; Nakamura, H.; Kimura, T. Low-field magnetoelectric effect at room temperature. *Nat. Mater.* **2010**, *9*, 797–802.
14. Soda, M.; Ishikura, T.; Nakamura, H.; Wakabayashi, Y.; Kimura, T. Magnetic Ordering in Relation to the Room-Temperature Magnetoelectric Effect of $Sr_3Co_2Fe_{24}O_{41}$. *Phys. Rev. Lett.* **2011**, *106*, 087201.
15. Kumar, K.; Mishra, S.K.; Singh, S.; Baev, I.; Martins, M.; Orlandi, F.; Manuel, P.; Pandey, D. Evidence for Conical Magnetic Structure in M-Type $BaFe_{12}O_{19}$ Hexaferrite: A Combined Single-Crystal X-ray Magnetic Circular Dichroism and Neutron Diffraction Study. *Phys. Status Solidi (RRL)* **2021**, *15*, 2000506.
16. Ebnabbasi, K.; Mohebbi, M.; Vittoria, C. Room temperature magnetoelectric effects in bulk poly-crystalline materials of M-and Z-type hexaferrites. *J. Appl. Phys.* **2013**, *113*, 17C703.
17. Aleshko-Ozhevskii, O.P.; Sizov, R.A.; Cheparin, V.P.; Yazmin, I.I. Helicoidal Antiphase Spin Ordering in Hexagonal Ferrites with Magnetoplumbite Structure. *J. Exp. Theor. Phys. Lett.* **1968**, *7*, 207.
18. Wang, L.; Wang, D.; Cao, Q.; Zheng, Y.; Xuan, H.; Gao, J.; Du, Y. Electric control of magnetism at room temperature. *Sci. Rep.* **2012**, *2*, 223.
19. Ryu, J.; Carazo, A.V.; Uchino, K.; Kim, H.E. Magnetoelectric properties in piezoelectric and magnetostrictive laminate composites. *Jpn. J. Appl. Phys.* **2001**, *40*, 4948-4951.
20. Nan, C.W.; Bichurin, M.I.; Dong, S.; Viehland, D.; Srinivasan, G. Multiferroic magnetoelectric composites: Historical perspective, status, and future directions. *J. Appl. Phys.* **2008**, *103*, 031101.
21. Ortega, N.; Kumar, A.; Scott, J.F.; Katiyar, R.S. Multifunctional magnetoelectric materials for device applications. *J. Phys. Condens. Matter* **2015**, *27*, 504002.
22. Spaldin, N.A.; Ramesh, R. Advances in magnetoelectric multiferroics. *Nat. Mater.* **2019**, *18*, 203–212.
23. Liu, N.; Du, P.; Zhou, P.; Tanguturi, R.G.; Qi, Y.; Zhang, T. Magnetoelectric coupling in CoFe2O4-Pb (Zr0. 2Ti0. 8) O3 coaxial nanofibers. *J. Am. Ceram. Soc.* **2021**, *104*, 948–954.
24. Jiang, Q.H.; Shen, Z.J.; Zhou, J.P.; Shi, Z.; Nan, C.W. Magnetoelectric composites of nickel ferrite and lead zirconnate titanate prepared by spark plasma sintering. *J. Eur. Ceram. Soc.* **2007**, *27*, 279–284.
25. Bichurin, M.; Petrov, R.; Tatarenko, A. Magnetoelectric composites: Modeling and application. *Adv. Mater.* **2020**, *9*, 10–11648.
26. Bochenek, D.; Niemiec, P.; Brzezińska, D.; Dercz, G.; Ziółkowski, G.; Jartych, E.; Grotel, J.; Suchanicz, J. Magnetoelectric properties of multiferroic composites based on $BaTiO_3$ and nickel-zinc ferrite material. *Materials* **2024**, *17*, 1905.
27. Premkumar, S.; Mathe, V.L. Effect of co-sintering time on magnetoelectric response of $Pb_{0.895}Sr_{0.06}La_{0.03}(Zr_{0.56}Ti_{0.44})O_3$ multilayer-$Ni_{0.6}Zn_{0.4}Fe_2O_4$ composite fabricated by tape casting. *J. Appl. Phys.* **2019**, *126*, 084106.
28. Zhang, J.; Du, H.; Xia, X.; Fang, C.; Weng, G.J. Theoretical study on self-biased magnetoelectric effect of layered magnetoelectric composites. *Mech. Mater.* **2020**, *151*, 103609.
29. Deka, B.; Lee, Y.W.; Yoo, I.R.; Gwak, D.W.; Cho, J.; Song, H.C.; Choi, J.J.; Hahn, B.D.; Ahn, C.W.; Cho, K.H. Designing ferroelectric/ferromagnetic composite with giant self-biased magnetoelectric effect. *Appl. Phys. Lett.* **2019**, *115*, 192901.
30. Annapureddy, V.; Park, S.H.; Song, H.; Ryu, J. Tunable self-biased magnetoelectric effect in magnetization-graded magnetoelectric composites. *J. Alloys Compd.* **2023**, *957*, 170121.
31. Mathe, V.L.; Srinivasan, G.; Balbashov, A.M. Magnetoelectric effects in bilayers of lead zirconate titanate and single crystal hexaferrites. *Appl. Phys. Lett.* **2008**, *92*, 122505.
32. Saha, S.; Acharya, S.; Popov, M.; Sauyet, T.; Pfund, J.; Bidthanapally, R.; Jain, M.; Page, M.R.; Srinivasan, G. A Novel Spinel Ferrite-Hexagonal Ferrite Composite for Enhanced Magneto-Electric Coupling in a Bilayer with PZT. *Sensors* **2023**, *23*, 9815.
33. Jing, Y.; Jia, L.; Zheng, Y.; Zhang, H. Hydrothermal synthesis and competitive growth of flake-like M-type strontium hexaferrite. *RSC Adv.* **2019**, *9*, 33388–33394.
34. Urquhart, H.M.; Goldman, J.E. Magnetostrictive effects in an antiferromagnetic hematite crystal. *Phys. Rev.* **1956**, *101*, 1443.
35. Cullity, B.D.; C. D. Graham., *Introduction to Magnetic Materials*; John Wiley & Sons, Inc.: Hoboken, NJ, USA, 2009.
36. Hu, Z.; Stenning, G.B.; Koval, V.; Wu, J.; Yang, B.; Leavesley, A.; Wylde, R.; Reece, M.J.; Jia, C.; Yan, H. Terahertz faraday rotation of $SrFe_{12}O_{19}$ hexaferrites enhanced by Nb doping. *ACS Appl. Mater. Interfaces* **2022**, *14*, 46738–46747.

37. Liu, C.; Kan, X.; Hu, F.; Liu, X.; Feng, S.; Hu, J.; Wang, W.; Rehman, K.M.U.; Shezad, M.; Zhang, C.; et al. Characterizations of magnetic transition behavior and electromagnetic properties of Co-Ti co-substituted SrM-based hexaferrites $SrCo_xTi_xFe_{12-2x}O_{19}$ compounds. *J. Alloys Compd.* **2019**, *784*, 1175–1186.
38. Lechevallier, L.; Le Breton, J.M.; Teillet, J.; Morel, A.; Kools, F.; Tenaud, P. Mössbauer investigation of $Sr_{1-x}La_xFe_{12-y}Co_yO_{19}$ ferrites. *Phys. B Condens. Matter* **2003**, *327*, 135–139.
39. Williams, J.M.; Adetunji, J.; Gregori, M. Mössbauer spectroscopic determination of magnetic moments of Fe^{3+} and Co^{2+} in substituted barium hexaferrite, $Ba(Co,Ti)_xFe_{(12-2x)}O_{19}$. *J. Magn. Magn. Mater.* **2000**, *220*, 124–128.
40. Ustinov, A.B.; Tatarenko, A.S.; Srinivasan, G.; Balbashov, A.M.; Al substituted Ba-hexaferrite single-crystal films for millimeter-wave devices. *J. Appl. Phys.* **2009**, *105*, 023908.
41. Sheen, J. Comparisons of microwave dielectric property measurements by transmission/reflection techniques and resonance techniques. *Meas. Sci. Technol.* **2009**, *20*, 042001.
42. De Bitetto, D.J. Anisotropy fields in hexagonal ferrimagnetic oxides by ferrimagnetic resonance. *J. Appl. Phys.* **1964**, *35*, 3482–3487.
43. Zhuravlev, V.A.; Naiden, E.P.; Shestakov, A.S.; Erkaev, P.V. Ferromagnetic Resonance Spectra in Hexaferrites of $Sr(Co_xTi_x)Fe_{12-2x}O_{19}$ System Obtained by the SHS Method. *Russ. Phys. J.* **2013**, *55*, 1229–1231.
44. Sánchez, Y.; Briceño, S.; Larionova, J.; Long, J.; Guari, Y.; Silva, P. Temperature dependence of the ferromagnetic resonance (FMR) for $Mn_xCo_{1-x}Fe_2O_4$ ($0 \leq x \leq 1$) nanoparticles. *J. Mater. Res.* **2021**, *36*, 3329–3338.
45. Guerra, J.D.; Betal, S.; Pal, M.; Garcia, J.E.; Oliveira, A.J.; M'Peko, J.C.; Hernandes, A.C.; Guo, R.; Bhalla, A.S. Magnetoelectric response in $(1-x)PbZr_{0.65}Ti_{0.35}O_3$-$xBaFe_{12}O_{19}$ multiferroic ceramic composites. *J. Am. Ceram. Soc.* **2015**, *98*, 1542–1547.
46. Palneedi, H.; Maurya, D.; Kim, G.Y.; Priya, S.; Kang, S.J.L.; Kim, K.H.; Choi, S.Y.; Ryu, J. Enhanced off-resonance magnetoelectric response in laser annealed PZT thick film grown on magnetostrictive amorphous metal substrate. *Appl. Phys. Lett.* **2015**, *107*, 012904.
47. Ryu, J.; Priya, S.; Uchino, K.; Kim, H.E. Magnetoelectric effect in composites of magnetostrictive and piezoelectric materials. *J. Electroceram.* **2002**, *8*, 107–119.
48. Ryu, J.; Priya, S.; Carazo, A.V.; Uchino, K.; Kim, H.E.; Effect of the magnetostrictive layer on magnetoelectric properties in lead zirconate titanate/terfenol-D laminate composites. *J. Am. Ceram. Soc.* **2001**, *84*, 2905–2908.
49. Lu, S.G.; Jin, J.Z.; Zhou, X.; Fang, Z.; Wang, Q.; Zhang, Q.M. Large magnetoelectric coupling coefficient in poly (vinylidene fluoride-hexafluoropropylene)/Metglas laminates. *J. Appl. Phys.* **2011**, *110*, 104103.